PNAS

Supporting Information for

Hydrogen isotope fractionation is controlled by CO_2 in coccolithophore lipids

Ismael Torres-Romero[1*†], Hongrui Zhang[1*†], Reto S. Wijker[1], Alexander J. Clark[1], Rachel E. McLeod[1], Madalina Jaggi[1], Heather M. Stoll[1]

[1] Climate Geology, Department of Earth Sciences, ETH Zürich, Sonneggstrasse 5, 8092 Zurich, Switzerland

† These two authors contributed equally to this work.

*Corresponding authors: Ismael Torres-Romero and Hongrui Zhang

Email: ismael.torres@erdw.ethz.ch, zhh@ethz.ch

This PDF file includes:

Other supporting materials for this manuscript include the following:

SI Materials and methods

1. Laboratory measurements

1.1. Cell concentration, size and growth rate.

After thorough resuspension of the photobioreactor vessel, 1 mL of culture was harvested at least once per day for cell growth monitoring at the same hour. A Multisizer 4e particle counter and sizer (Beckman Coulter) measured cell concentration and mean cell diameter. Growth rate (μ) was measured from cell concentrations in intervals of 24 h to account for entire day/night cycles. In turbidostat, μ equals dilution rate (D) and was calculated by the following equations:

$$\mu = \mathrm{D} + \frac{\ln X_1 - \ln X_0}{t_1 - t_0} \quad (1)$$

$$\mathrm{D} = \frac{V_O + V_H}{V_{PBR}(t_1 - t_0)} \quad (2)$$

where X_0 is cell concentration at time 0 (t_0), X_1 is cell concentration at time 1 day (t_1), V_0 is outflow volume, V_H is harvested volume, and V_{PBR} is the photobioreactor vessel liquid volume.

1.2. Carbonate system and aeration.

Culture medium for photobioreactor experiments was K/2 (1) made with artificial seawater (ASW) (2) without Tris buffer and supplemented with $NaHCO_3$ and HCl to yield an initial dissolved inorganic carbon (DIC) of 2 mM or 4 mM. Calculations of the carbonate system were based on pH and DIC, using the NBS scale, 35‰ salinity, 7 µM phosphate and 0 µM silicate, in the CO2SYS excel macro (3).

With an internal pH-probe integrating a temperature sensor (InPro 3253SG/120/PT1000, Mettler Toledo), pH was continuously monitored and checked externally for harvested samples with a pH-meter (FiveEasy, Mettler Toledo) calibrated with NIST buffer standards (Mettler Toledo).

Concentrations of DIC were measured during cell harvesting and at least once the day before. After external pH measurement, cells were spun down and culture seawater supernatant was analyzed for DIC. In duplicate, 3.5 mL were measured with an Apollo SciTech DIC-C13 Analyzer coupled to a Picarro CO_2 analyzer calibrated with Dickson standard #186 and in-house $NaHCO_3$ aqueous solutions of known concentrations. The Apollo-Picarro instrument had an analytical error of 10 µM for DIC.

Photobioreactors and fresh media were pre-bubbled and bubbled throughout the experiment to achieve carbonate chemistry equilibrium. Gas CO_2 concentrations were measured with the Picarro CO_2 analyzer and corrected with certified gas mixtures of known ppm (PanGas and Air Liquide). Different air and CO_2 mixtures from 200 to 2000 ppm were bubbled into the photobioreactor system. To adjust CO_2 concentrations, first, our source of compressed air went through an NDC-140 CO_2 scrubber (F-DGSi) to obtain clean CO_2-free air. Then this air was mixed with our in-house pure CO_2 bottle using a Gas Mixing System (GMS 150, Photon Systems Instruments). The flow was split and Mass Flow Controllers (Vögtlin Instruments) regulated the bubbling flow rate at 50 to 100 mL min^{-1}.

Flow first entered the fresh media bottle prior to a gas filter (0.2 µm). The bottle was bubbled from the bottom to humidify the gas and equilibrate fresh media. Then gas collected at the bottle headspace went through a bubble-interrupting valve delimited by two additional filters whose role was to interrupt flow into the photobioreactor vessel for a few seconds every minute to avoid bubble interference during OD680 readings. Gas was directed into a U-shaped sparger at the bottom of the vessel. Gas accumulating at the vessel headspace exited through the outflow tubing shared with the liquid outflow. Gas flow left the system from the outflow bottle headspace.

1.3. Chlorophyll analysis.

About 10^6-10^7 cells were harvested from photobioreactors in duplicate. Cells were pelleted at 4000 *g* for 5 min and supernatant discarded before snap-freezing in N_2 (l) and stored at -20°C. Pellets were thoroughly resuspended in 1 mL pure methanol and transferred to 1.5 mL tubes. Pigment extraction was allowed for at least 1 h to overnight at -20°C. Tubes were centrifuged for 5 min at 11000 *g* and supernatants were transferred into polystyrene cuvettes for spectrophotometer readings at 470, 652.4, 665.2 and 750 nm. The following empirical formula was used to quantify chlorophyll (4):

$$Chlorophyll\ \left(\frac{\mu g}{mL}\right) = 19.71(Abs652.4 - Abs750) + 4.44(Abs665.2 - Abs750) \quad (3)$$

1.4. Elemental analysis (EA) of particulate organic carbon and nitrogen (POC and PON).

In precombusted quartz fiber filters (QM-A, Whatman), 50 mL of cultures were filtered and snap-frozen in N_2 (l). With an acid-base reaction, the inorganic carbon from samples was removed by converting $CaCO_3$ into CO_2 (g). This was achieved by placing the filters inside a desiccator and exposing them to acid fumes issued from 50 mL of a 6% H_2SO_3 solution. A vacuum pump was stopped below 20 mbar to evaporate the acid, and the desiccator was closed to allow acid vapors to react for at least 24 h before reopening it, which changed pigment color. Filters were further dried overnight at 60°C, compacted with a press and wrapped into tin cups with a pair of tweezers. Wrapped filter pellets were combusted in a ThermoFisher Flash-EA 1112 coupled with a Conflo IV interface to a ThermoFisher Delta V-IRMS, and carbon and nitrogen concentrations were quantified against known standards.

1.5. Particulate inorganic carbon (PIC) determination.

In polycarbonate membranes (Whatman Cyclopore), 20 mL of culture were filtered in triplicate. The seawater flowthrough was discarded and the cells on the filter were further washed with MQ-water before storing at -20°C. Calcite on membranes was dissolved immersing in 1 mL of 2% HNO_3 and vortexing well. Filter and cell debris were spun down (11000 *g*, 2 min) and 400 µL of clear supernatant containing the dissolved calcium ions were transferred into Teflon tubes for analysis by inductively coupled plasma mass spectrometry (Agilent 8800 ICP-QQQ-MS). PIC was calculated from the molar concentration of Ca as $CaCO_3$ per cell.

1.6. Lipid extraction and derivatization.

Cells from 100-200 mL of *G. oceanica* were harvested at least in duplicate in precombusted glass fiber filters, then snap-frozen and stored at -20°C. The total lipid fraction was extracted and quantified using an isopropanol and methyl tert-butyl ether (MTBE) protocol (5). Filters were unfrozen by addition of 1 mL preheated isopropanol containing 0.01% butylated hydroxytoluene for protection against double bond oxidation. Pellets were homogenized by vortexing and sonication and immediately heated at 85°C for 10 min to lyse cells and inactivate lipases. After cooling down to room temperature, 10 µg of standard C27:0 alkenone (14-heptacosanone), triacylglycerol C17:C17:C17 (TAG) and 5-α-cholestane (all Sigma) were added to account for extraction yield and lipid quantification. Three mL of MTBE were added before vortexing. Phase separation was possible by mixing with 1 mL water and centrifuging for 5 min at 3200 *g*. Upper organic phase free of cell debris and filter was transferred to a clean glass tube. Higher extraction yield was achieved by re-extracting with an additional 1 mL MTBE and pooling the organic phases. In a bath up to 30°C and under a gentle N_2 (g) stream, organic solvents were evaporated. Lipids were redissolved in methanol/chloroform (1:2, v/v) and half of the sample was transferred into a vial and dried again to redissolve in hexane or toluene for GC analysis of alkenones.

The remaining half was evaporated as well and 2 mL of methanol with 5% H_2SO_4 were added for lipid transmethylation. Conversion of acyl-lipids into fatty acid methyl esters (FAME) occurred in glass vials for at least 1h at 85°C ensuring they were leak-tight along the incubation. After cooling down, phase separation was obtained by adding 1 mL water 0.9% NaCl (w/v) and 500 µL hexane, vortexing well and centrifuging for 5 min at 3200 *g*. The upper hexane phase was transferred into a GC vial without taking any acid.

1.7. Lipid identification and quantification.

The alkenones and fatty acids extracted and derivatized from continuous cultures were analyzed by a gas chromatography (GC) equipped with a programmable temperature vaporization injector (PTV) and coupled to a flame ionization detector (FID). Samples were injected with a TriPlus RSH Autosampler in splitless mode. Helium gas with a flow rate of 1.5 ml min^{-1} was used as the carrier gas. Chromatographic separation of alkenones was achieved with a 60 m x 0.25 mm capillary column (VF-200ms, 0.25 µm film thickness, Agilent) and a 5 m x 0.25 mm guard column (Agilent) with the following temperature program: 1 min at 120°C and temperature gradient of 40°C min^{-1} to 200°C, 5°C min^{-1} to 300°C, then hold for 15 min, then to 320°C with 10°C min^{-1} and hold for 1 min. Chromatographic separation of FAMEs was carried out with a 30 m x 0.32 mm capillary column (Rtx-Wax, 0.5 µm film thickness, Restek) and the following GC program: 2 min at 50°C and temperature gradient of 15°C min^{-1} to 150°C, 6°C min^{-1} to 240°C, then hold for 5 min. Peaks were identified by comparing retention times with an in-house alkenone standard in-house alkenone standard (provided by G. O'Neil (Western Washington University) and C. M. Reddy (Woods Hole Oceanographic Institution) and FAME standards (Marine oil FAME Mix, Restek #35066), respectively. Peak areas of unknown analytes were compared with that of an internal standard (C27:0 alkenone or C17:0 FAME) that was added to the sample before lipid extraction.

2. Statistical analysis.

In **Fig. 1**, for the 50 and 100 µE condition, CO_2 concentrations define only two endmembers. While we report the sensitivity to CO_2 using a simple linear regression model, we cannot rule out nonlinear (e.g. logarithmic or other) relationships between these endmembers. Prism version 10 was used to calculate multiple linear regression with least squares for **Table S1**. For **Fig. S5**, Pearson correlations coefficients and two-tailed *p*-values for every pair of variables were computed with Prism software.

3. Numerical model.

The stable hydrogen isotope ratio of alkenones was modeled with the cellular flows and their associated H fractionations hypothesized in the Discussion section. MathWorks MATLAB version R2021b was used to develop the model and ordinary differential equation (ODE) solver 'ode15s', for simulations. All the metabolic fluxes taken into account are summarized in a model diagram (**Fig. 3A**) and defined in **Table S4**.

The model is built upon the fate of the hydrogen atoms from NADPH, intracellular water and alkenone precursors, all determining alkenone α. The first assumption is that the only source of NADPH is ferredoxin:$NADP^+$ reductase (FNR) enzyme transferring the electrons from photosystem I to NADPH (light-dependent reaction) in the chloroplast, and that NADPH generation is the most significant isotope fractionation step. Other sources such as the oxidative pentose phosphate pathway (oxPPP) or the citric acid cycle (TCA) in cytosol and transport of hydrogen through the chloroplast membrane via a malate (or a C3 or C4) shuttle are not simulated in this model.

3.1. Generation of NADPH

The generation rate of NADPH in the chloroplast is driven by the following equations:

$$F_1 = V_{max,1} \frac{\mathrm{h}\nu}{K_{M1,light} + \mathrm{h}\nu} \frac{[NADP]}{K_{M1,NADP} + [NADP]} \quad (4)$$

$$V_{max,1} = k_{vmax,1} V_{max,CBB} \quad (5)$$

In Eq. 4, the first flux F_1 is described as a Michaelis-Menten equation where V_{max} is the maximum velocity at saturating substrate concentrations and the K_M are the Michaelis constants or the substrate concentrations at which the reaction velocity is half of the V_{max}. The hν is the light intensity with a unit of µE. To emulate natural conditions, in our culture setup the light follows a sinusoidal curve during the photoperiod (**Fig. S3**). To simplify our simulation, here all hν are set to the daily maximum values in our

model. The [NADP] is the concentration of $NADP^+$, which can be calculated as $Pool_N$ – [NADPH] – [NADPD]. [NADPH] and [NADPD] are the concentrations of NADPH and NADPD (the accepted ^1H is replaced by ^2H).

In our model, all V_{max} of NADPH-related process are anchored with maximum reaction rate of CBB using a constant, k, such as the $k_{vmax,1}$ in Eq. 5. The constant k is fitted using the measured hydrogen isotope data. In theory, the fluxes of a Michaelis-Menten process can be tuned by both V_{max} and K_M. Neither the V_{max} or K_M in the NADPH-related reactions can be found in literature. Thus, to reduce the degrees of freedom of our model and achieve a higher efficiency in parameter fitting, the K_M is set as the maximum NADPH/NADP concentration in chloroplast, considering the NADP amount is the main limitation in high light environment. Similar settings can also be found in the calculation of NADPH exchange and NADPH consumption in carbon fixation (**Table S5**).

Then, the generation rate of NADPD can be calculated from the total flux of NADPH considering percentage of deuterium in water and isotopic fractionation:

$$F_{1D} = F_1 \frac{p_{W,x}}{2} \alpha_{N-W,1} \quad (6)$$

In Eq. 6, $p_{W,x}$ is the fraction of HDO in all water molecules in the chloroplast compartment (subindex x) and the $\frac{p_{W,x}}{2}$ is the fraction of deuterium in all hydrogen atoms. All the parameter descriptions are compiled in **Table S5**.

Similarly, the generation rate of NADPH (pure NADPH without any deuterium) can be calculated based on mass balance as follows:

$$F_{1H} = F_1 - F_{1D} \quad (7)$$

3.2. Exchange of hydrogen between NADPH and water

The second flux F_2 illustrates the hydrogen exchange between NADPH and water in a reaction catalyzed by enzymes such as glutathione reductase (GR). This process follows also a Michaelis-Menten kinetics, the rate of which depends on the enzyme GR concentration and turnover rate ($V_{max,2}$), the substrates concentrations and their half-saturation concentration ($K_{M,2}$). The function of GR is to maintain the cellular redox balance by catalyzing the reduction of oxidized glutathione (GSSG) to its reduced form (GSH) using NADPH as a cofactor. This process helps to protect cells from oxidative stress by scavenging reactive oxygen species (ROS) and maintaining the antioxidant capacity of the cell, particularly at high light to avoid light-induced damage (6). Thus, light intensity would trigger the cell to upregulate (1) GR expression and/or (2) its activity by increasing the production rate of NAPDH. Both of these two effects would result in a faster exchange between NADPH and water, and thereby a smaller fractionation between water and alkenone. Here, to reduce the degrees of freedom of the model, we combine these two effects into the NADPH producing, and assume the exchanging between water and NADPH + NADPD is always in balance. Thus, the hydrogen flux from water to NADPH(D) ($F_{2,W2N}$) is equal with flux from NADPH(D) to water ($F_{2,N2W}$):

$$F_2 = F_{2,N2W} = F_{2,W2N} = V_{max,2} \frac{[NADPH] + [NADPD]}{K_{M,2} + [NADPH] + [NADPD]} \quad (8)$$

Similar to the quantification of NADPH and NADPD fluxes in Section 3.1, the exchanging fluxes of two isotopes can be calculated by the following equations:

$$F_{2D,N2W} = F_2 \frac{[NADPD]}{[NADPH] + [NADPD]} \alpha_{W-N,2} \quad (9)$$

$$F_{2H,N2W} = F_2 - F_{2D,N2W} \quad (10)$$

$$F_{2H,W2N} = F_2 \frac{p_{W,x}}{2} \alpha_{N-W,2} \quad (11)$$

$$F_{2H,W2N} = F_2 - F_{2D,W2N} \quad (12)$$

3.3. Consumption of NADPH in carbon fiixatioin and lipid synthesis

The third flux F_3 is the carbon fixation via the Calvin-Benson-Bassham (CBB) cycle in the chloroplast. This step is controlled by the CO_2(aq) at the rubisco site, i.e. the chloroplast, [CO_{2x}], and consumes NADPH:

$$F_3 = V_{max,3} \frac{[CO_{2x}]}{K_{M,3} + [CO_{2x}]} \quad (13)$$

In Eq. 13, [CO_{2x}] can be estimated by the [CO_{2sw}], CO_2(aq) of seawater, and a carbon concentrating mechanism (CCM) factor: [CO_{2x}] = k_{CCM} [CO_{2sw}]. The $V_{max,3}$ can be calculated by the rubisco amount and turnover rate of rubisco at a temperature T.

$$V_{max,3} = N_{Rubisco}\, k_{cat\_Rubisco} \quad (14)$$

There is a significant temperature effect on growth rate of coccolithophore. Here we assume this temperature effect plays a role in H isotope fractionation by controlling rubisco turnover rate, $k_{cat_{Rubisco}}$, which can be described as:

$$k_{cat_{Rubisco}} = 2.67\left(k_T\left(T - T_{opt}\right)^2 + 1\right) \quad (15)$$

In Eq. 15, the 2.67 s^{-1} is the turnover rate of rubisco at optimal temperature (T_{opt}) for coccolithophore growth (7).

Similarly, the fluxes of NADPH with two different isotopes can be calculated separately:

$$F_{3D} = F_3 \frac{[NADPD]}{[NADPH] + [NADPD]} \alpha_{N-C,3} \quad (16)$$

$$F_{3H} = F_3 - F_{3D} \quad (17)$$

The fourth flux is the lipid synthesis by the fatty acid synthetase (FAS) system. Here we assume alkenones are produced in two phases: an initial phase in the chloroplast where NADPH and the CBB metabolites produce C16 fatty acids (F_4), and a later phase in the cytoplasm where the C16 fatty acid is exported outside the chloroplast and is further elongated by the same FAS enzymes and same substrates up to a C37 alkenone ($F_{4'}$). This presumes at least half of the hydrogens in alkenones are from outside the chloroplast.

$$F_4 = F_3\, R_{C16-CBB} \quad (18)$$

$$F_{4D} = F_4 \frac{[NADPD]}{[NADPH] + [NADPD]} \alpha_{N-L,4} \quad (19)$$

$$F_{4H} = F_4 - F_{4D} \quad (20)$$

$$F_{4'} = F_4\, R_{C37-C16} \quad (21)$$

$$F_{4'D} = F_{4'} \frac{[NADPD]}{[NADPH] + [NADPD]} \alpha_{N-L,4} \quad (22)$$

$$F_{4'H} = F_{4'} - F_{4'D} \quad (23)$$

The fifth flux F_5 describes the water exchange rate in the chloroplast and can be calculated from the water amount in the chloroplast W_x and water residence time $\tau_{W,x}$:

$$F_{5,in} = \frac{W_x}{\tau_{W,x}} \tag{24}$$

$$F_{5,out} = F_{5,in} - F_1 - R_{W-CBB}F_3 - R_{W-C16}F_4 \tag{25}$$

$$F_{5D,in} = F_{5,in}p_{W,x} \tag{26}$$

$$F_{5D,out} = F_{5,out}p_{W,c} \tag{27}$$

In Eq. 27, $p_{W,c}$ is the fraction of HDO in all water molecules in the cytoplasm (subindex c).

3.4. Ordinary differential equations (ODEs) for NADPH concentrations and water amount

The concentration of NADPH, NADPD and amount of HDO in chloroplast can be calculated by resolving the following ODEs:

$$\frac{d[NADPH]}{dt} = \frac{1}{vol}\left(F_{1H} + F_{2H,W2N} - F_{2H,N2W} - R_{N-CBB}F_{3H} - R_{N-C16}F_{4H}\right) \tag{28}$$

$$\frac{d[NADPD]}{dt} = \frac{1}{vol}\left(F_{1D} + F_{2D,W2N} - F_{2D,N2W} - R_{N-CBB}F_{3D} - R_{N-C16}F_{4D}\right) \tag{29}$$

$$\frac{\mathrm{d}HDO_x}{dt} = -F_{1D} + F_{2D,N2W} - F_{2D,W2N} - R_{W-CBB}F_{3D} - R_{W-C16}F_{4D} + F_{5D,in} - F_{5D,out} \tag{30}$$

It should be noted here that the F_3, F_4 and $F_{4'}$ are based on carbon fluxes and have a unit of mol C s^{-1}. To calculate the hydrogen fluxes, the hydrogen ratios of NADPH-flux ($R_{N\text{-}C3}$, $R_{N\text{-}C16}$, $R_{N\text{-}C37}$) and water-flux ($R_{W\text{-}CBB}$, $R_{W\text{-}C16}$) should be employed in equations 28-30. The volume of chloroplast, vol, can be calculated as proposed by McClelland et al. (2017) (8).

3.5. Alkenone hydrogen isotope ratio

The hydrogen isotope of NADPH and water in chloroplast can be calculated as:

$$R_{NADPH,x} = \frac{[NADPD]}{[NADPH]} \tag{31}$$

$$R_{W,x} = \frac{HDO_x}{2\,H_2O_x + HDO_x} \tag{32}$$

In Eq. 32, H_2O_x is the amount of water with only ^1H, and is calculated from the compartment volume as follows:

$$H_2O_x = 0.7\,\frac{1000}{18}vol - HDO_x \tag{33}$$

where 0.7 is the proportion of the chloroplast volume occupied by water, 18 g mol^{-1} is the molar mass of water and 1000 g L^{-1} is the density of water.
Then, the isotope ratio of C3 can be determined from the hydrogen isotope of water and NADPH in chloroplast:

$$R_{C3} = \frac{P_{C3,Nx}\,\frac{R_{N,x}}{1+R_{N,x}} + P_{C3,Wx}\,\frac{R_{W,x}}{1+R_{W,x}}}{1 - \left(P_{C3,Nx}\,\frac{R_{N,x}}{1+R_{N,x}} + P_{C3,Wx}\,\frac{R_{W,x}}{1+R_{W,x}}\right)} \tag{34}$$

Similarly, the isotope ratio of C16 can be calculated from the mixing of C3, NADPH and water in chloroplast:

$$R_{C16} = \frac{P_{C16,C3}\,\frac{R_{C3}}{1+R_{C3}} + P_{C16,Nx}\,\frac{R_{N,x}}{1+R_{N,x}} + P_{C16,Wx}\,\frac{R_{W,x}}{1+R_{W,x}}}{1-\left(P_{C16,C3}\,\frac{R_{C3}}{1+R_{C3}} + P_{C16,Nx}\,\frac{R_{N,x}}{1+R_{N,x}} + P_{C16,Wx}\,\frac{R_{W,x}}{1+R_{W,x}}\right)} \quad (35)$$

Finally, isotope ratio of C37 can be calculated from the mixing of C16, NADPH and water in cytoplasm:

$$R_{C37} = \frac{P_{C37,C16}\,\frac{R_{C16}}{1+R_{C16}} + P_{C37,Nc}\,\frac{R_{N,c}}{1+R_{N,c}} + P_{C37,Wc}\,\frac{R_{W,c}}{1+R_{W,c}}}{1-\left(P_{C37,C16}\,\frac{R_{C16}}{1+R_{C16}} + P_{C37,Nc}\,\frac{R_{N,c}}{1+R_{N,c}} + P_{C37,Wc}\,\frac{R_{W,c}}{1+R_{W,c}}\right)} \quad (36)$$

The δ^2H_{C37} is calculated by:

$$\delta^2\mathrm{H}_{C37} = \left(\frac{\mathrm{R}_{C37}}{\mathrm{R}_{VSMOW}} - 1\right) \times 1000 \quad (37)$$

And the fractionation of C37 and water, $\alpha_{C37\text{-}W}$, can be calculated by Eq. 4 as described above, which is the apparent alkenone hydrogen isotope fractionation measured in experiments ($\alpha_{alkenone}$).

3.6. NADPH residence time in chloroplast

The key mechanism proposed in this work is the NADPH residence time in the chloroplast, which can be calculated as follows:

$$\tau_{NADPH,x} = \frac{[NADPH_x]}{F_1 + F_2} \quad (38)$$

where the $[NAPDH_x]$ is the concentration of NADPH in chloroplast (including both NADPH and NADPD). For mass balance, we have F1 = F3+F4. Thus, by combining the equation (5), (13), (18) and (21), the $[NAPDH_x]$ can be calculated as following equation 39:

$$[NADPH_x] = \frac{V_{max,3}[CO_{2x}]K_{M1,NADP}(1 + R_{N-CBB}R_{C16-CBB})}{V_{max,1}\left(K_{M3,CO2} + [CO_{2x}]\right)\mathrm{h\nu} - V_{max,3}\,[CO_{2x}](1 + R_{N-CBB}R_{C16-CBB})\left(K_{M31,Light} + \mathrm{h\nu}\right)} \quad (39)$$

Combining the equation 38 and 39, we obtain:

$$\tau_{NADPH,x} = \frac{[NADPH_x]}{V_{max,1}\frac{\mathrm{h\nu}}{K_{M1,Light} + \mathrm{h\nu}}\,\frac{Pool_N - [NADPH_x]}{K_{M1,NADP+} + Pool_N - [NADPH_x]} + V_{max,2}\frac{[NADPH_x]}{K_{M2} + [NADPH_x]}} \quad (40)$$

3.7. Simulation caveats

It should be noted that the predictions of α_{C37} at a given temperature, light and CO_2(aq) in this model did not match perfectly with the measurements (with Pearson linear correlation r = 0.75, **Fig. S11**). The difference between the simulation and measurements are mainly caused by four aspects:

(1) We employed a fixed CCM intensity, in which the chloroplast CO_2(aq) is always as 1.5 times of the culture media CO_2(aq). The CCM intensity is not well constrained at present, but with help of alkenone carbon isotope fractionations, it would hopefully simulate better the CCM process in further works.

(2) The KIE in different reactions have been poorly studied so far. To simplify, we assumed that most of fractionations happen in the generation of NADPH.

(3) We did not simulate the NADPH generation in chloroplast by other pathways due to lack of information. Also, the NADPH can be exchanged between chloroplast and cytoplasm, which can change the $NADPH_x$ and $NADPH_c$ in the model.

(4) The water hydrogen isotope ratios in cytoplasm was fixed as same as seawater. If the cytoplasm water has a much long resident time (>100 s), there could be up to 20 ‰ isotopic shift, which might partly explain the difference between our simulations and measurements.

Supplementary Figures

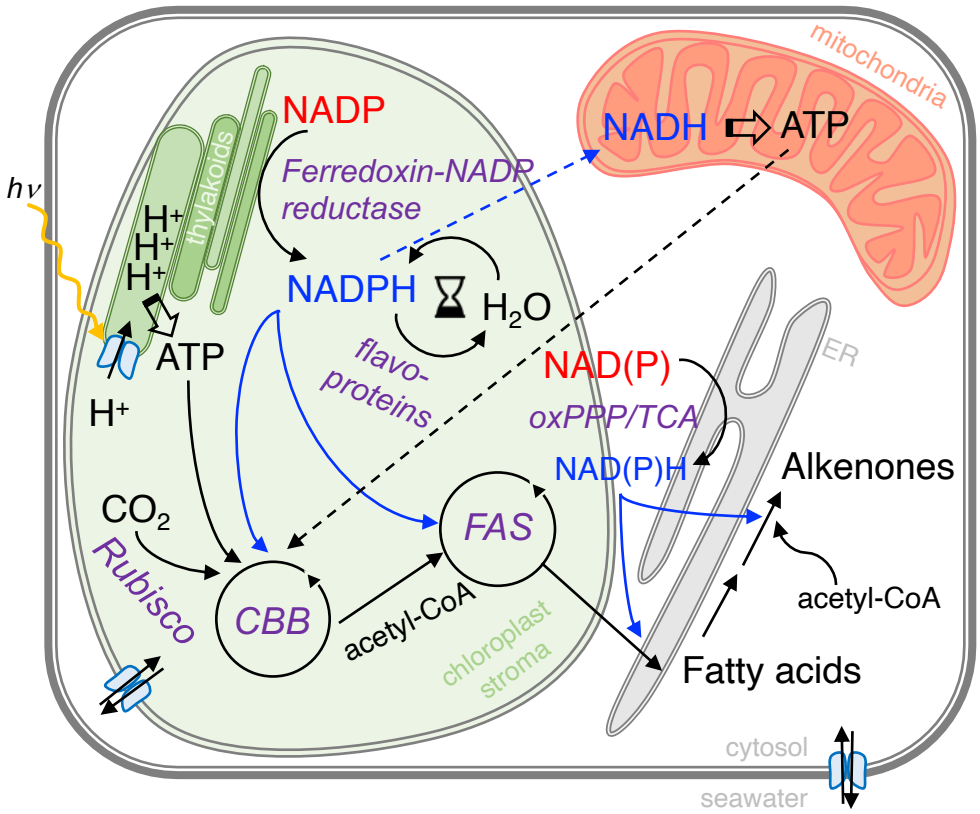

Fig. S1. Cell model showing alkenone biosynthesis and the fluxes affecting H isotopic signature. The ferredoxin-NADP reductase introduces a δ^2H in NADPH of -600‰ relative to the stromal water. This ^{2}H-depleted H from NADPH exchanges with the intracellular ^{2}H-enriched water via flavoproteins. Stromal NADPH is mainly consumed by the Calvin-Benson-Bassham cycle (CBB) and the fatty acid synthetase (FAS) complex, whose competition with flavoproteins determines NADPH residence time. The CBB produces C3 compounds that can generate acetyl-CoA for fatty acid production by the FAS. These fatty acids can be exported to the endoplasmic reticulum (ER) and cytosol for further elongation to produce alkenones. Other sources of NAD(P)H introduce a less negative δ^2H such as the oxidative Pentose Phosphate Pathway (oxPPP) or the tricarboxylic acid cycle (TCA). The different H_2O channels and pumps influence the water δ^2H in each compartment. As biomass is depleted in deuterium, intracellular water is enriched, especially in the stroma, where light-activated H^+ pumps generating the H^+ gradient fueling ATP synthesis could further affect δ^2H fractionation.

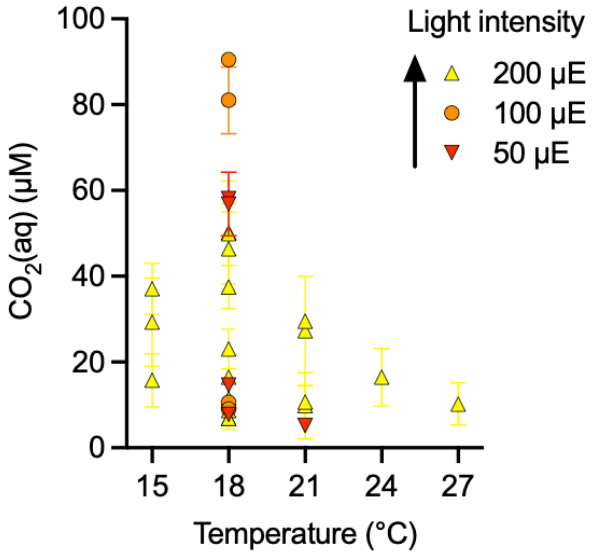

Fig. S2. Matrix of growth conditions for *G. oceanica* continuous culture samples (*N* = 29).

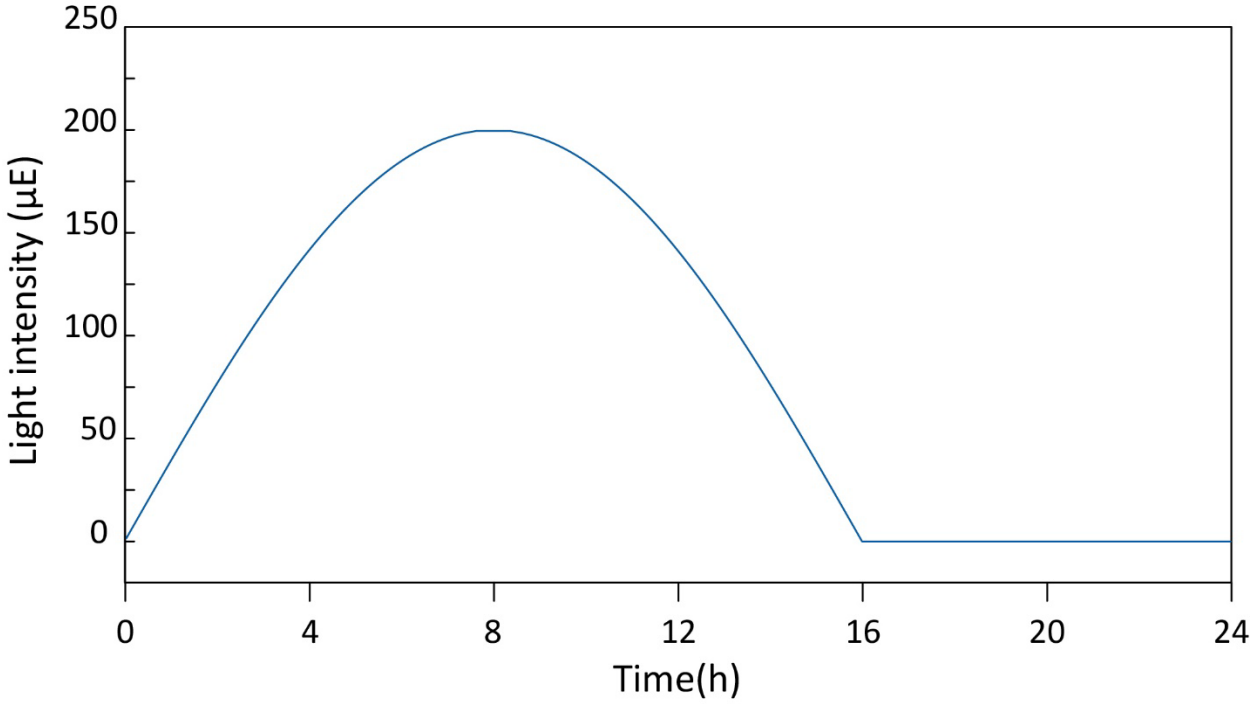

Fig. S3. Variation of light intensity during a day-night cycle for 200 μE experiments.

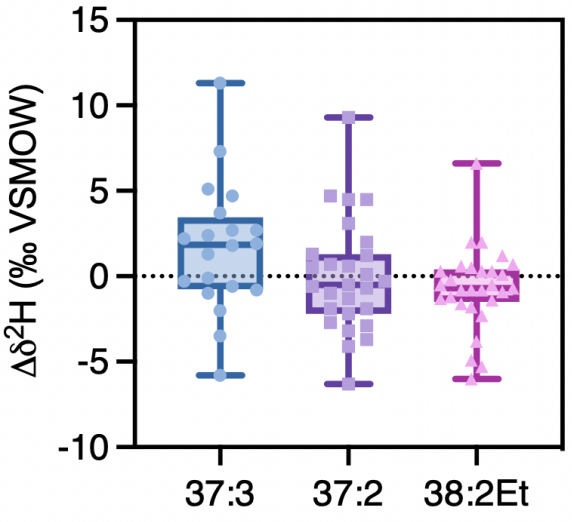

Fig. S4. Differences between δ^2H of each individual alkenone from the weighted average of the three alkenones for that sample. Boxplot shows the distribution of compound-specific δ^2H variation for all the cultures (*N* = 29) with overlaid datapoints representing each an average of technical replicates.

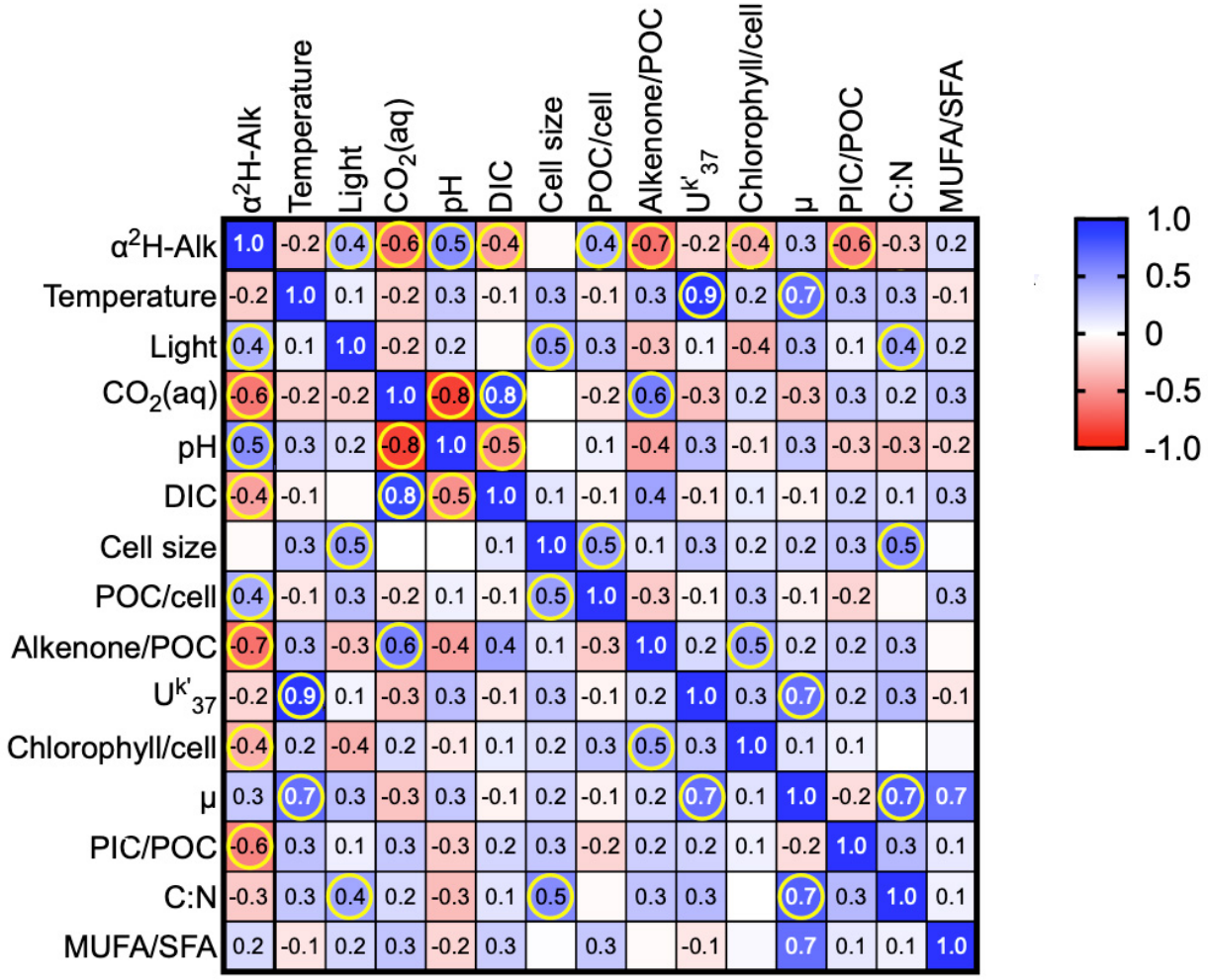

393
394
395 **Fig. S5. Heat map of the correlation matrix indicating Pearson correlation coefficients.** Pairs whose
396 two-tailed *p*-value is <0.05 are highlighted in yellow circles. Abbreviations: α^2H-Alk, hydrogen isotope
397 fractionation between alkenones and water; DIC, dissolved inorganic carbon; POC, particulate organic
398 carbon; μ, growth rate; PIC, particulate inorganic carbon; C:N, carbon/nitrogen ratio; MUFA/SFA,
399 monounsaturated to saturated fatty acids ratio.

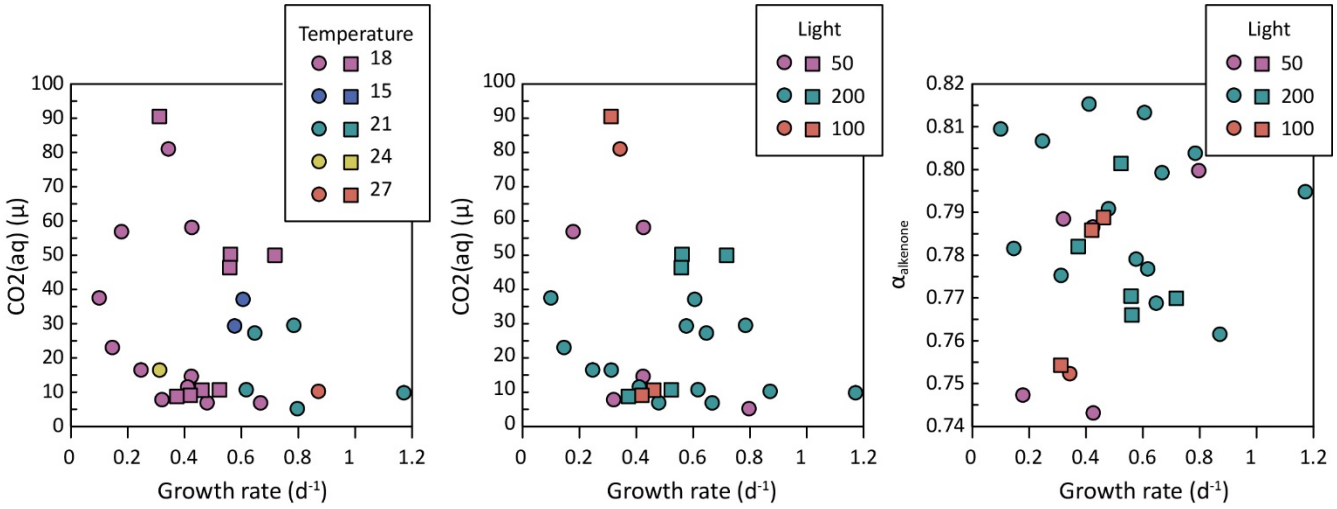

Fig. S6. Cross-plots between growth rate, CO_2(aq) and alkenone hydrogen isotope fractionation ($\alpha_{alkenone}$) in this work. Color code indicates temperature or light intensity. Circles represent growth rates estimated by optical density and squares represent those estimated by cell counting.

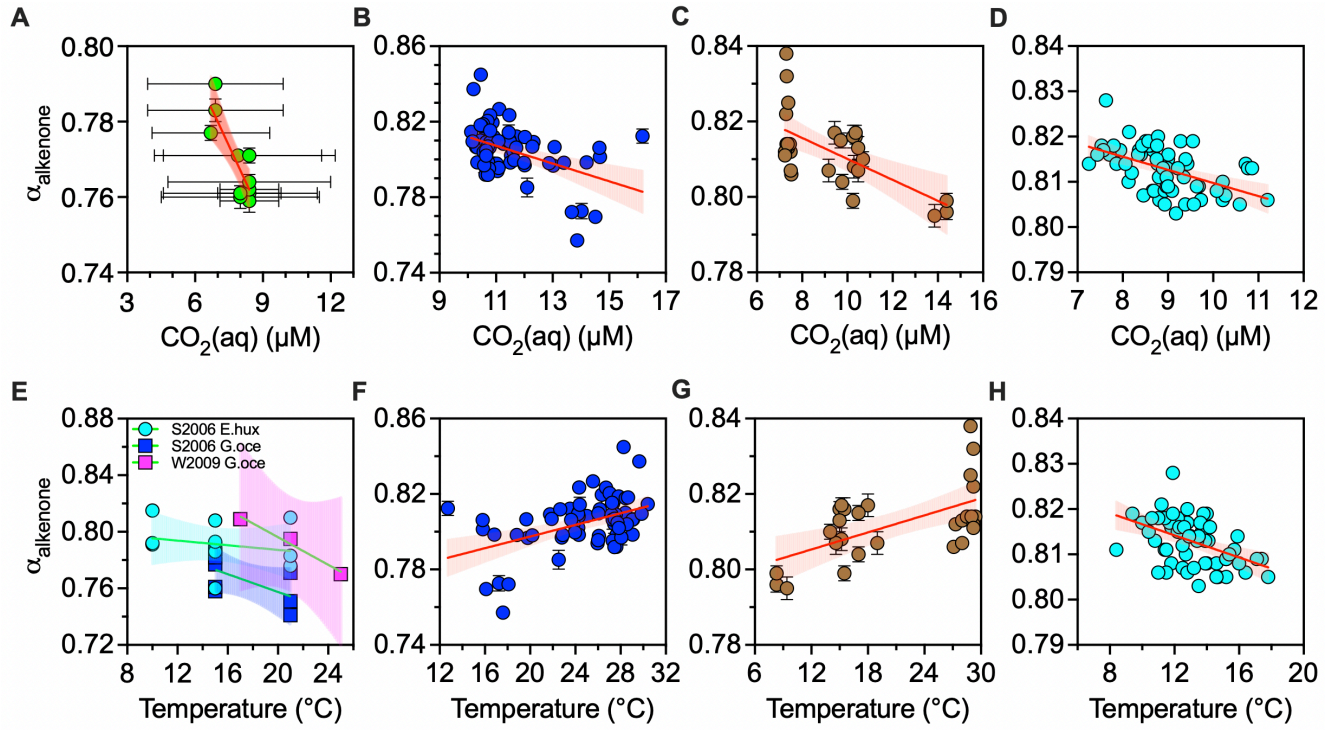

Fig. S7. Slope regressions from previous cultures and environmental data used in Fig. 2. (**A-D**) Alkenone α in function of estimated CO_2(aq) or (**E-H**) in function of temperature. (**A**) From Weiss et al. (2019) cultures (9) excluding Exp. 6. (**E**) S2006 E.hux are *E. huxleyi* cultures and S2006 G.oce are *G. oceanica* cultures from Schouten et al. (2006) (10), and W2009 *G.oce* are also *G. oceanica* cultures from Wolhowe et al. (2009) (11). (**B, F**) SPOM samples from Gould et al. (2019) (12). (**C, G**) Core-tope samples from Weiss et al. (2019) (13). (**D, H**) Glacial-interglacial samples from the Chile margin (14).

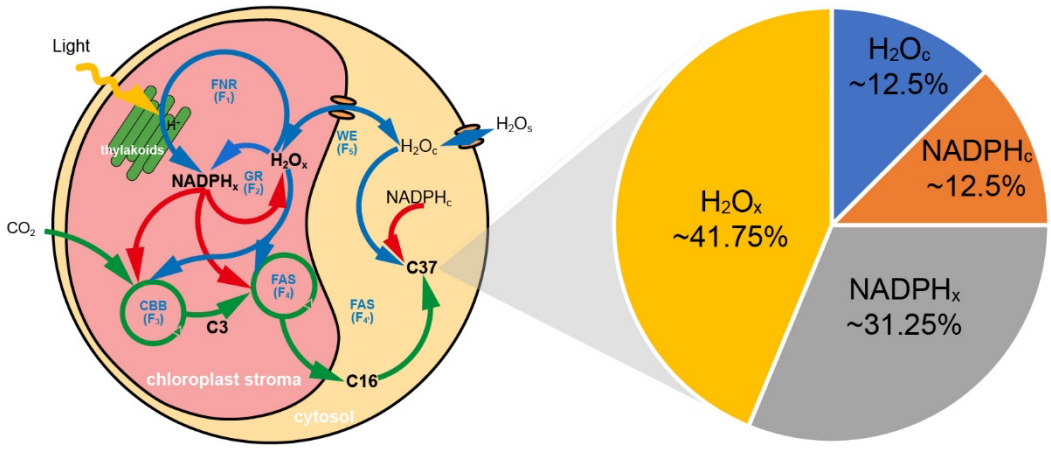

Fig. S8. Proposed hydrogen source of alkenones as simulated in this study, detailed in Methods. Left panel illustrates the main fluxes as labeled in Figure 3, and right panel indicates the relative contributions of H to the alkenones.

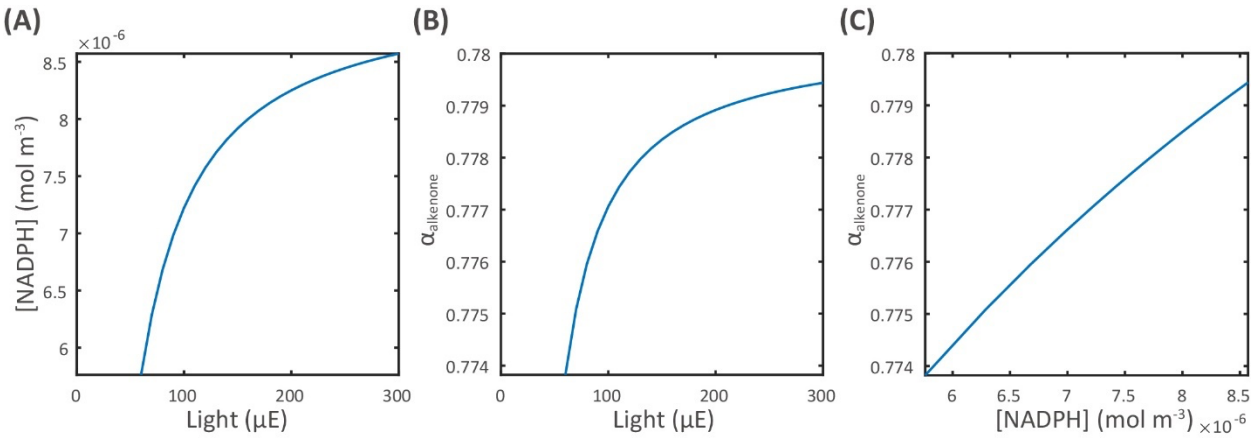

Fig. S9. Sensitivity tests of hydrogen isotope fractionation ($\alpha_{alkenone}$) on light at 20 μM CO_2(aq). (**A**) The NADPH concentration in chloroplast increases at higher light intensities. (**B**) The $\alpha_{alkenone}$ increases at higher light intensities. (**C**) The $\alpha_{alkenone}$ increases with NADPH concentration.

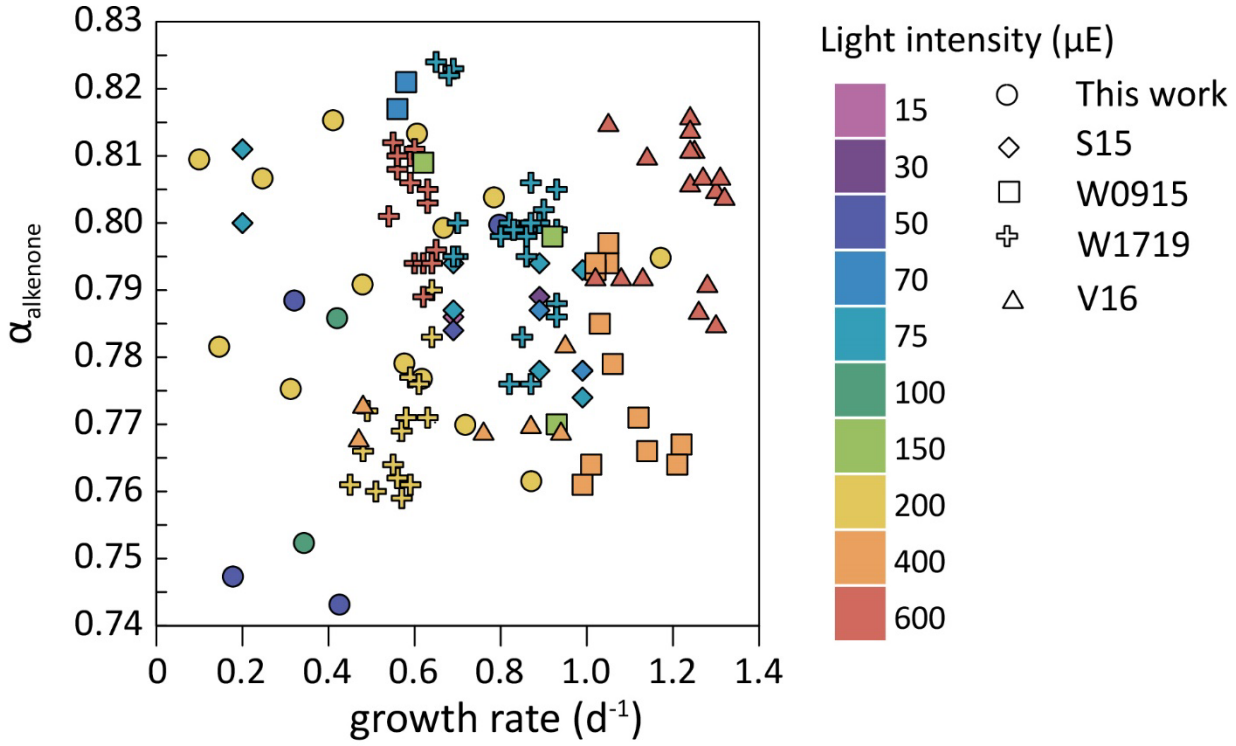

Fig. S10. Cross-plot of growth rate and alkenone hydrogen isotope fractionation ($\alpha_{alkenone}$) in this work and in other published datasets. S15 represents Sachs and Kawaka, 2015 (15); W0915 represents Wolhowe et al., 2009 and 2015 (11, 16); W1719 is Weiss et al., 2017 and 2019 (17, 9); V16 is van der Meer et al., 2015 (18).

436

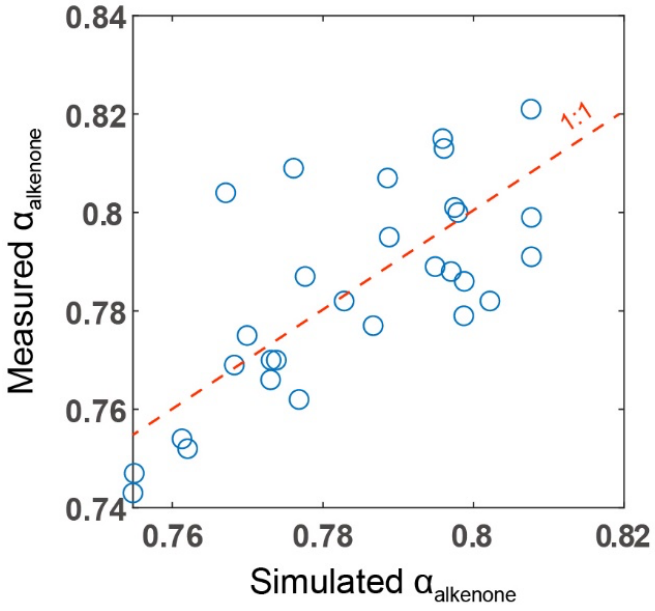

437

438 **Fig. S11. Comparison between simulated hydrogen isotope fractionation ($\alpha_{alkenone}$) and**
439 **measurements from laboratory cultures.**

Supplementary Tables

Table S1. Culture conditions in 29 experiments used in this study.

Experiment	Light (µE)	Temperature (°C)	$[CO_2(aq)]$ (µM)	Experiment	Light (µE)	Temperature (°C)	$[CO_2(aq)]$ (µM)
1	50	18	14.6	16	200	21	27.3
2	100	18	10.6	17	200	24	16.4
3	100	18	9.1	18	200	27	10.2
4	200	18	8.7	19	200	18	16.5
5	200	18	10.7	20	200	18	37.5
6	200	18	11.5	21	200	18	6.9
7	50	18	58.1	22	200	15	37.1
8	50	18	56.9	23	200	15	15.7
9	100	18	90.5	24	200	21	9.8
10	100	18	81	25	200	21	29.5
11	200	18	50.2	26	50	21	5.2
12	200	18	46.4	27	200	21	10.7
13	200	18	49.9	28	200	18	6.9
14	200	15	29.3	29	50	18	7.8
15	200	18	23				

Table S2. Comparison of multiple linear regression results. From #1 to #6, the MLR are carried out by using the different combinations of parameters with a form of $\alpha_{alkenone} = \sum_1^n (k_i \times x_i) + b$, where k is the slope of each parameter in the column of "estimate", x is the parameter and b is the intercept. It should be noted that the combination #6 can best predict the $\alpha_{alkenone}$. However, these parameters describe the coccolithophores response to the environmental drivers and, in this work, our target is linking the environment variations with $\alpha_{alkenone}$. Thus, in the main text, we only discuss the #1 and #2, which give the best prediction on how environmental variations drives $\alpha_{alkenone}$.

MLR	Parameters	Estimate	Standard Error	P value	R^2
α_{alk} #1	Intercept	0.8526	0.0223	<0.0001	**0.6153**
	Temperature	$-3.566 \cdot 10^{-3}$	$1.074 \cdot 10^{-3}$	0.0028	(*N*=29)
	Light	$8.815 \cdot 10^{-5}$	$4.326 \cdot 10^{-5}$	0.0523	
	CO_2(aq)	$-6.017 \cdot 10^{-4}$	$1.187 \cdot 10^{-4}$	<0.0001	
α_{alk} #2	Intercept	0.8807	0.02639	<0.0001	**0.5854**
	Temperature	$-3.714 \cdot 10^{-3}$	$1.124 \cdot 10^{-3}$	0.0029	(*N*=29)
	Light	$1.258 \cdot 10^{-4}$	$4.387 \cdot 10^{-5}$	0.0083	
	log(CO_2aq)	$-3.672 \cdot 10^{-2}$	$7.819 \cdot 10^{-3}$	<0.0001	
α_{alk} #3	Intercept	0.8668	0.02249	<0.0001	0.5496
	Temperature	$-3.480 \cdot 10^{-3}$	$1.138 \cdot 10^{-3}$	0.0051	(*N*=29)
	CO_2(aq)	$-6.531 \cdot 10^{-4}$	$1.228 \cdot 10^{-4}$	<0.0001	
α_{alk} #4	Intercept	0.7844	0.01016	<0.0001	0.4453
	Light	$8.366 \cdot 10^{-5}$	$5.088 \cdot 10^{-5}$	0.1122	(*N*=29)
	CO_2(aq)	$-5.127 \cdot 10^{-4}$	$1.362 \cdot 10^{-4}$	0.0009	
α_{alk} #5	Intercept	0.8061	0.02835	<0.0001	0.2209
	Temperature	$-2.355 \cdot 10^{-3}$	$1.460 \cdot 10^{-3}$	0.1189	(*N*=29)
	Light	$-1.365 \cdot 10^{-4}$	$5.889 \cdot 10^{-5}$	0.0286	
α_{alk} #6	Intercept	0.8206	0.0076	<0.0001	**0.8459**
	Alkenone/POC	-0.5135	0.1462	0.0049	(*N*=15)
	PIC/POC	$-4.171 \cdot 10^{-2}$	$1.163 \cdot 10^{-2}$	0.0043	
	MUFA/SFA	$3.032 \cdot 10^{-2}$	$8.910 \cdot 10^{-3}$	0.0059	

Table S3. Estimation of CO_2 effect on $\alpha_{alkenone}$ in our cultures and in previously published culture, SPOM, and sediment data. Abbreviations: MLR, multiple linear regression; N, number of datapoints; SE, standard error; SST, sea surface temperature; SSS, sea surface salinity.

Study	CO_2(aq) calculation	Data selection	Slope	SE	*N*
Our cultures 18°C, 50 µE	From pH and DIC. CO_2(aq) is the average of previous 3 days of cultivation.		$-8.99 \cdot 10^{-4}$	$9.89 \cdot 10^{-5}$	**18**
Our cultures 18°C, 100 µE			$-4.46 \cdot 10^{-4}$	$6.85 \cdot 10^{-5}$	12
Our cultures 18°C, 200 µE			$-5.14 \cdot 10^{-4}$	$1.56 \cdot 10^{-4}$	46
Our cultures all conditions (MLR)			$-6.02 \cdot 10^{-4}$	$1.19 \cdot 10^{-4}$	29
Cultures *E. huxleyi* RCC2050 (Weiss et al. 2019) (9)	From initial and final pH and total alkalinity. Plotted CO_2(aq) is average of initial and final.	Excluded cultures with greater than 5 µM variation in CO_2(aq) between initial and final. Experiment 6 excluded due to much smaller alkalinity drawdown (<200 µM) compared to Exp. 1-5 suggests differences in culture growth.	Without Exp.6: -0.0126 With exp. 6 -0.0017	Without Exp.6: $2.65 \cdot 10^{-3}$ With Exp. 6: 0.0019	Without Exp.6: 11 With Exp.6: 12
SPOM (Gould et al. 2019) (12)	Assuming modern 400 ppm and air-sea equilibrium for the salinity and temperature.		-0.00471	0.00115	69
Core-tops (Weiss et al. 2019 GCA) (13)	Assuming pre-industrial 280 ppm and air-sea equilibrium for the salinity and temperature.	Included only samples from regions of alkenone production dominated by *E. huxleyi* and *Gephyrocapsa spp.* (Baltic samples excluded).	-0.00278	$6.66 \cdot 10^{-4}$	28
Glacial-Interglacial (Weiss et al. 2019 PP) (14)	With estimations of atmospheric pCO_2 from ice core (19) and assuming air-sea equilibrium with alkenone SST and modern SSS.		-0.0029	$6.20 \cdot 10^{-4}$	64

Table S4. Summary of metabolic fluxes constraining alkenone $^{2}H/^{1}H$ ratio. In this table, F_{nH} is the flux for the molecules with ^{1}H and F_{nD}, for ^{2}H (D).

Metabolic fluxes	Definition
F_1, F_{1H}, F_{1D}	Generation rate of NADPH by ferredoxin:$NADP^+$ reductase (FNR) with the electrons from light-dependent water splitting
F_2, F_{2H}, F_{2D}	Exchanging rate of NADPH with water in chloroplast via glutathione reductase (GR)
F_3, F_{3H}, F_{3D}	Carbon fixing rate in Calvin-Benson-Bassham (CBB) cycle
F_4, F_{4H}, F_{4D}	Lipid synthesis flux controlled by the fatty acid synthetase (FAS) system
F_5, F_{5H}, F_{5D}	Water exchanging flux between chloroplast and cytoplasm

460 **Table S5. Parameters in the model, their definitions, derivation and units.**

461

Symbol	Definition	Derivation	Quantity	Unit
Measured parameters				
r	Cell radius	Measured directly	Variable	m
$h\nu$	Light intensity	Measured directly	Variable	μmol m^{-2} s^{-1}
T	Growth temperature	Measured directly	Variable	°C
CO_{2sw}	CO_2 concentration in culture medium	Measured [DIC] and pH	Variable	μmol L^{-1}
$\alpha_{alkenone-water}$	Hydrogen isotope fractionation (α) between alkenones and water	Measured $\delta^2H_{alkenone}$ and δ^2H_{water}	Variable	ratio
Parameters from literature				
k_{ccm}	CCM factor (ratio of CO_2 concentration in chloroplast and seawater)	CO_{2x}/CO_{2sw}	1.5	ratio
$k_{cat,Rubisco}$	Turnover rate of rubisco	From Cummins et al. (2018) (20)	Eq. 17 (2.67 at 25°C)	s^{-1}
$Pool_N$	NADPH and $NADP^+$ concentrations	From Tanaka et al. (2021) (21)	1×10^{-5}	mol m^{-3}
$\rho_{RubisCO}$	Rubisco density	From Zhang et al. (2021) (22)	1.3×10^{-17}	m^{-3}
T_{opt}	Optimal temperature of *G. oceanica*	Inferred from Buitenhuis et al. (2008) (7)	30	°C
$K_{M1,Light}$	Half saturation constant of light in NADPH generation (F_1)	Inferred from Krumhardt et al. (2017) (23)	200	μmol m^{-2} s^{-1}
$K_{M3,CO2}$	Half saturation constant of CO_2 in CBB cycle (F_1)	From Heureux et al. (2017) (24)	18	μmol L^{-1}
$\alpha_{W-N,x}$	α between NADPH and water during NADPH synthesis in chloroplast	Inferred from Sachs et al. (2016) (25)	0.3	ratio
$\alpha_{W-N,c}$	α between NADPH and water during NADPH synthesis in cytoplasm	Inferred from Sachs et al. (2016) (25)	0.6	ratio
$\alpha_{W-N,2}$, $\alpha_{N-W,2}$	α between NADPH and water during exchange ($\alpha_{W-N,2} = 1/\alpha_{N-W,2}$)	Inferred from Sachs et al. (2016) (25)	1.0	ratio
$\alpha_{N-C,3}$	α between NADPH and C3 during Calvin-Benson cycle	Inferred from Sachs et al. (2016) (25)	1.0	ratio
$\alpha_{N-L,4}$	α between NADPH and lipid during lipid synthesis	Inferred from Sachs et al. (2016) (25)	1.0	ratio
$\alpha_{W-L,4}$	α between water and lipid during lipid synthesis	Inferred from Sachs et al. (2016) (25)	1.0	ratio
R_{N-CBB}	Ratio of NADPH consumption rate and CBB rate	Inferred from Sharkey (2021) (26)	1.0	ratio
R_{N-C16}	Ratio of NADPH consumption rate and lipid synthesis rate	Inferred from FAS (Baan et al. 2023) (27)	2.0	ratio

$R_{W\text{-}CBB}$	Ratio of water consumption rate and CBB rate	Fixing 1 mol carbon in CBB, 2 mol hydrogen will be added and 2/3 of them are from water.	4/3	ratio
$R_{W\text{-}C16}$	Ratio of water consumption rate and lipid synthesis rate	Extending 1 mol carbon in lipid, 2 mol hydrogen will be added and 25% of them are from water.	0.5	ratio
$R_{C16\text{-}CBB}$	Ratio of lipid synthesis rate and CBB rate	Inferred from lipid dry weight in cell from Aveiro et al. (2020) (28)	0.17	ratio
$P_{C3,Wx}$, $P_{C3,Nx}$	Hydrogen contribution of chloroplast water (W_x), chloroplast NADPH (N_x) to C_3	Inferred from Baan et al. (2023) (27)	66.7, 33.3	%
$P_{C16,Wx}$, $P_{C16,Nx}$, $P_{C16,C3}$	Hydrogen contribution of chloroplast water (W_x), chloroplast NADPH (N_x) and C_3 to lipids (C_{16})	Inferred from Baan et al. (2023) (27)	25, 25, 50	%
$P_{C37,Wc}$, $P_{C37,Nc}$, $P_{C37,lipid}$	Hydrogen contribution of cytoplasm water (W_c), cytoplasm NADPH (N_c) and lipid (C_{16}-C_{18}) to alkenone (C_{37})	Inferred from Baan et al. (2023) and Rontani et al. (2006) (27) (27, 29)	12.5, 12.5, 75	%
Fitted parameters				
$k_{vmax,1}$	Ratio of $V_{max,1}$ and $V_{max,CBB}$ (at optimal temperature)	Fitted, $V_{max,1} = k_{vmax,1} \times V_{max,CBB}$	3.1696	ratio
$k_{vmax,2}$	Ratio of $V_{max,exchange}$ and $V_{max,CBB}$ (at opt temperature)	Fitted, $V_{max,2} = k_{vmax,2} \times V_{max,CBB}$	0.9287	ratio
k_T	Temperature constant for k_{cat}	Fitted	-2.4361	ratio
$K_{M1,NADP+}$	Half saturation constant of NADP+ in NADPH generation (F_1)	Inferred	$1\times Pool_N$	mol
$K_{M2,NADPH}$	Half saturation constant of NADPH in NADPH-water exchange (F_2)	Inferred	$1\times Pool_N$	mol
$K_{M3,NADPH}$	Half saturation constant of NADPH in CBB (Reaction 3)	Inferred	$0.2\times Pool_N$	mol
$\tau_{W,X}$	Water residence time in chloroplast	Inferred, minor role in hydrogen isotope ratios	1×10^{-5} ~ 1×10^{-1}*	s

*The optimization of parameters was carried out with $\tau_{W,X}$ = 0.1 s.

Dataset S1. Culture data.

Abbreviations: Alk, alkenone; α^2H, alpha, hydrogen isotope fractionation between lipids and water; FA, fatty acid; DIC, dissolved inorganic carbon; POC, particulate organic carbon; μ, growth rate; PIC, particulate inorganic carbon; C:N, carbon/nitrogen ratio; MUFA/SFA, monounsaturated to saturated fatty acids ratio.

SI References

1. M. D. Keller, R. C. Selvin, W. Claus, R. R. L. Guillard, Media for the culture of oceanic ultraphytoplankton. *Journal of Phycology* **23**, 633–638 (1987).
2. D. R. Kester, I. W. Duedall, D. N. Connors, R. M. Pytkowicz, Preparation of Artificial Seawater. *Limnology and Oceanography* **12**, 176–179 (1967).
3. D. Pierrot, E. Lewis, D. W. R. Wallace, MS Excel program developed for CO_2 system calculations (CO2sys_v2.3xls). Carbon Dioxide Information Analysis Center (CDIAC), Oak Ridge National Laboratory, U.S. Department of Energy, Oak Ridge, TN. (2006). https://doi.org/10.3334/CDIAC/otg.CO2SYS_XLS_CDIAC105a. Deposited 2006.
4. H. K. Lichtenthaler, [34] Chlorophylls and carotenoids: Pigments of photosynthetic biomembranes. *Methods in Enzymology* **148**, 350–382 (1987).
5. B. Légeret, *et al.*, Lipidomic and transcriptomic analyses of *Chlamydomonas reinhardtii* under heat stress unveil a direct route for the conversion of membrane lipids into storage lipids. *Plant, Cell & Environment* **39**, 834–847 (2016).
6. S. J. Müller-Schüssele, *et al.*, Chloroplasts require glutathione reductase to balance reactive oxygen species and maintain efficient photosynthesis. *The Plant Journal* **103**, 1140–1154 (2020).
7. E. T. Buitenhuis, T. Pangerc, D. J. Franklin, C. Le Quéré, G. Malin, Growth rates of six coccolithophorid strains as a function of temperature. *Limnology and Oceanography* **53**, 1181–1185 (2008).
8. H. L. O. McClelland, J. Bruggeman, M. Hermoso, R. E. M. Rickaby, The origin of carbon isotope vital effects in coccolith calcite. *Nature Communications* **8**, 14511 (2017).
9. G. M. Weiss, *et al.*, Hydrogen isotope fractionation response to salinity and alkalinity in a calcifying strain of *Emiliania huxleyi*. *Organic Geochemistry* **134**, 62–65 (2019).
10. S. Schouten, *et al.*, The effect of temperature, salinity and growth rate on the stable hydrogen isotopic composition of long chain alkenones produced by *Emiliania huxleyi* and *Gephyrocapsa oceanica*. *Biogeosciences* **3**, 113–119 (2006).
11. M. D. Wolhowe, F. G. Prahl, I. Probert, M. Maldonado, Growth phase dependent hydrogen isotopic fractionation in alkenone-producing haptophytes. *Biogeosciences* **6**, 1681–1694 (2009).
12. J. Gould, M. Kienast, M. Dowd, E. Schefuß, An open-ocean assessment of alkenone δD as a paleo-salinity proxy. *Geochimica et Cosmochimica Acta* **246**, 478–497 (2019).
13. G. M. Weiss, S. Schouten, J. S. Sinninghe Damsté, M. T. J. van der Meer, Constraining the application of hydrogen isotopic composition of alkenones as a salinity proxy using marine surface sediments. *Geochimica et Cosmochimica Acta* **250**, 34–48 (2019).
14. G. M. Weiss, *et al.*, Paleosensitivity of Hydrogen Isotope Ratios of Long-Chain Alkenones to Salinity Changes at the Chile Margin. *Paleoceanography and Paleoclimatology* **34**, 978–989 (2019).
15. J. P. Sachs, O. E. Kawka, The influence of growth rate on $^2H/^1H$ fractionation in continuous cultures of the coccolithophorid *Emiliania huxleyi* and the diatom *Thalassiosira pseudonana*. *PLOS ONE* **10**, e0141643 (2015).
16. M. D. Wolhowe, F. G. Prahl, G. Langer, A. M. Oviedo, P. Ziveri, Alkenone δD as an ecological indicator: A culture and field study of physiologically-controlled chemical and hydrogen-isotopic variation in C37 alkenones. *Geochimica et Cosmochimica Acta* **162**, 166–182 (2015).
17. G. M. Weiss, E. Y. Pfannerstill, S. Schouten, J. S. Sinninghe Damsté, M. T. J. van der Meer, Effects of alkalinity and salinity at low and high light intensity on hydrogen isotope fractionation of long-chain alkenones produced by *Emiliania huxleyi*. *Biogeosciences* **14**, 5693–5704 (2017).
18. M. T. J. van der Meer, *et al.*, Large effect of irradiance on hydrogen isotope fractionation of alkenones in *Emiliania huxleyi*. *Geochimica et Cosmochimica Acta* **160**, 16–24 (2015).
19. P. Köhler, C. Nehrbass-Ahles, J. Schmitt, T. F. Stocker, H. Fischer, A 156 kyr smoothed history of the atmospheric greenhouse gases CO_2, CH_4, and N_2O and their radiative forcing. *Earth System Science Data* **9**, 363–387 (2017).

20. P. L. Cummins, B. Kannappan, J. E. Gready, Directions for Optimization of Photosynthetic Carbon Fixation: RuBisCO's Efficiency May Not Be So Constrained After All. *Frontiers in Plant Science* **9** (2018).
21. K. Tanaka, *et al.*, Quantification of NAD(P)H in cyanobacterial cells by a phenol extraction method. *Photosynth Res* **148**, 57–66 (2021).
22. H. Zhang, *et al.*, An isotope label method for empirical detection of carbonic anhydrase in the calcification pathway of the coccolithophore Emiliania huxleyi. *Geochimica et Cosmochimica Acta* **292**, 78–93 (2021).
23. K. M. Krumhardt, N. S. Lovenduski, M. D. Iglesias-Rodriguez, J. A. Kleypas, Coccolithophore growth and calcification in a changing ocean. *Progress in Oceanography* **159**, 276–295 (2017).
24. A. M. C. Heureux, *et al.*, The role of Rubisco kinetics and pyrenoid morphology in shaping the CCM of haptophyte microalgae. *J Exp Bot* **68**, 3959–3969 (2017).
25. J. P. Sachs, A. E. Maloney, J. Gregersen, C. Paschall, Effect of salinity on $^{2}H/^{1}H$ fractionation in lipids from continuous cultures of the coccolithophorid Emiliania huxleyi. *Geochimica et Cosmochimica Acta* **189**, 96–109 (2016).
26. T. D. Sharkey, Pentose Phosphate Pathway Reactions in Photosynthesizing Cells. *Cells* **10** (2021).
27. J. Baan, M. Holloway-Phillips, D. B. Nelson, A. Kahmen, The metabolic sensitivity of hydrogen isotope fractionation differs between plant compounds. *Phytochemistry* **207**, 113563 (2023).
28. S. S. Aveiro, *et al.*, The Polar Lipidome of Cultured Emiliania huxleyi: A Source of Bioactive Lipids with Relevance for Biotechnological Applications. *Biomolecules* **10**, 1434 (2020).
29. J.-F. Rontani, F. G. Prahl, J. K. Volkman, Re-Examination of the Double Bond Positions in Alkenones and Derivatives: Biosynthetic Implications1. *Journal of Phycology* **42**, 800–813 (2006).